Radical Cation Probes for Photoinduced Intramolecular Electron Transfer in Metal−Organic Complexes

Yingsheng Wang and Kirk S. Schanze*

Department of Chemistry, University of Florida, P.O. Box 117200, Gainesville, Florida 32611

Received: November 17, 1995[⊗]

Two transition metal complexes of the type *fac*-(bpy)$Re^{I}(CO)_3(DA)^+$ (where bpy = 2,2′-bipyridine and DA is a pyridine ligand that is substituted with a 1,2-diamine electron donor) have been prepared. The 1,2-diamine serves as a "reactive donor ligand" owing to its propensity to undergo rapid C−C bond fragmentation when activated by single electron transfer oxidation. Photoexcitation of the diamine complexes affords a ligand-to-ligand charge transfer (LLCT) state via intramolecular electron transfer quenching of a metal-to-ligand charge transfer (MLCT) state, $[(bpy)Re^{I}(CO)_3(DA)]^+ + h\nu \rightarrow [(bpy^{\bullet-})Re^{II}(CO)_3(DA)]^{+}$*(MLCT) → $[(bpy^{\bullet-})Re^{I}(CO)_3(DA^{\bullet+})]^{+}$*(LLCT). Photochemical product and quantum efficiency studies indicate that the diamine reactive donor ligand undergoes photoinduced C−C bond fragmentation with high efficiency, presumably via the radical cation ($DA^{\bullet+}$) which is present in the LLCT excited state. Laser flash photolysis allows direct detection of the metal complex based radicals that are formed by C−C bond fragmentation. Quantitative kinetic information gathered through luminescence, laser flash photolysis, and quantum yield studies allows estimation of the rates for formation of the LLCT state by forward electron transfer (k_{FET}), decay of the LLCT state by back electron transfer (k_{BET}), and the rate of diamine radical cation bond fragmentation in the LLCT state (k_{BF}). The relationship between these kinetic parameters and the driving force for electron transfer and bond fragmentation as well as the structure of the reactive donor ligands is discussed.

Introduction

Transition metal complexes have played a prominent role during the development of photoinduced electron transfer (ET).[1−6] Recently, research on photoinduced ET in transition metal systems has emphasized charge separation and recombination in metal complex "dyads" and "triads" that are festooned with organic electron donor and/or acceptor groups.[7−12] The study of these dyads and triads has led to increased understanding of the factors that control the efficiency for formation and lifetime of charge-separated ligand-to-ligand charge transfer (LLCT) states that are formed by ET between an organic donor−acceptor pair that are bridged by a transition metal center.

Our group has been examining the properties of LLCT excited states in transition metal complexes that feature diimine acceptor ligands such as 2,2′-bipyridine and a variety of organic amine donor ligands.[12] Through this effort we have developed complexes that undergo photochemistry from the LLCT state through the use of "reactive donor ligands" that are designed to undergo a rapid bond fragmentation reaction triggered by single ET oxidation (Scheme 1).[13] We have demonstrated that since the bond fragmentation reaction occurs from the LLCT state and must compete with charge recombination via back ET, detailed study of the efficiency of the permanent photochemical reaction affords insight concerning the dynamics of the forward and back ET reactions.[13]

Recently, we presented a detailed study of a series of complexes of the type *fac*-$[(bpy)Re^{I}(CO)_3(AA)]^+$, where bpy = 2,2′-bipyridine and AA is a reactive donor ligand which features the 1,2-aminoalcohol unit.[13a] These complexes were designed on the basis of previous reports which indicated that aminoalcohol radical cations undergo rapid C−C bond fragmentation, eq 1, X = OH:[14]

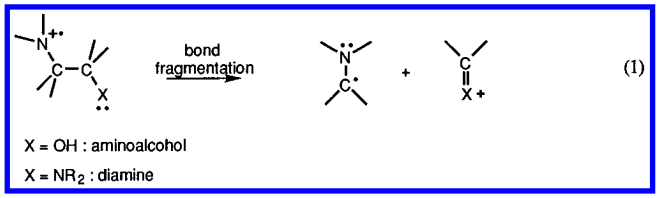

(1)

As anticipated on the basis of the reactivity of aminoalcohol radical cations, near-UV irradiation of two $[(bpy)Re^{I}(CO)_3(AA)]^+$ complexes led to C−C bond fragmentation of the aminoalcohol reactive donor ligand, albeit with low quantum efficiency.[13a] The C−C bond fragmentation reaction of the aminoalcohol moiety was presumed to occur via the LLCT state that is formed by forward ET quenching of the dπ (Re) → π* (bpy) metal-to-ligand charge transfer (MLCT) excited state,

$$[(bpy)Re^{I}(CO)_3(AA)]^+ + h\nu \rightarrow$$

$$*[(bpy^{\bullet-})Re^{II}(CO)_3(AA)]^+ \rightarrow \text{MLCT}$$

$$*[(bpy^{\bullet-})Re^{I}(CO)_3(AA^{\bullet+})]^+ \rightarrow \text{LLCT}$$

$$\text{bond fragmentation products} \quad (2)$$

While the $[(bpy)Re^{I}(CO)_3(AA)]^+$ complexes clearly demonstrated the utility of using a reactive donor ligand to probe the dynamics of the LLCT state, the aminoalcohol system was limited because the C−C bond fragmentation reaction of the aminoalcohol radical cation is comparatively slow ($k_{BF} \approx 10^5$−10^6 s^{-1}) and therefore does not compete effectively with decay of the LLCT state by back ET ($k_{BET} \approx 10^8$ s^{-1}).[13a] The comparatively slow rate of C−C bond fragmentation of the aminoalcohol cation radical was believed to be the reason that

⊗ Abstract published in *Advance ACS Abstracts,* March 1, 1996.

0022-3654/96/20100-5408$12.00/0

SCHEME 1

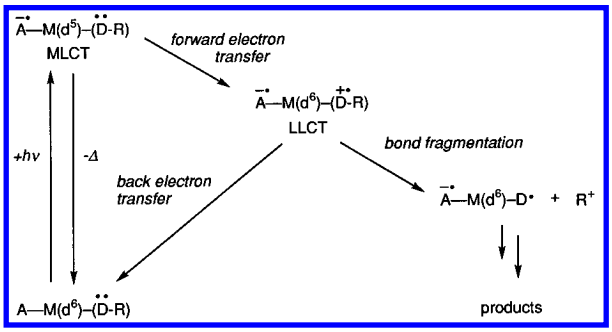

the overall quantum efficiency for reaction of the $[(bpy)Re^{I}(CO)_3(AA)]^+$ complexes was low.

More recently we have turned our attention to the photochemistry and photophysics of complexes of the type $[(bpy)Re^{I}(CO)_3(DA)]^+$, where DA is a 1,2-diamine reactive donor ligand.[13b,c] The decision to change from the aminoalcohol to the diamine reactive donor ligand was predicated by studies of bimolecular photoinduced ET which implied that C−C bond fragmentation in 1,2-diamine cation radicals (eq 1, X = NR_2) is substantially more rapid than in analogously substituted aminoalcohol radical cations.[15]

This report presents a detailed study of the photochemical and photophysical properties of ***e*-1a** and ***e*-1b** (Chart 1) that contain the *fac*-(bpy)$Re^{I}(CO)_3$-chromphore covalently linked to 1,2-diamine reactive donor ligands. Steady state photochemical studies demonstrate that photoexcitation of ***e*-1a** and ***e*-1b** into the dπ (Re) → π^* (bpy) MLCT absorption induces efficient C−C bond fragmentation of the diamine reactive donor ligand. Product studies also reveal that irradiation of ***e*-1a** and ***e*-1b** in degassed solution produces ***t*-1a** and ***t*-1b**, respectively, presumably via a mechanism involving reversible C−C bond fragmentation. Luminescence and nanosecond transient absorption studies indicate that (1) in both complexes formation of the LLCT state occurs rapidly ($k \geq 10^9\ s^{-1}$) after MLCT excitation; (2) C−C bond fragmentation occurs within the LLCT state with $k_{BF} \approx 3 \times 10^8\ s^{-1}$. Quantitative analysis of the steady state quantum yield data allows estimation of the rate of back ET to be $k_{BET} \approx 1 \times 10^8\ s^{-1}$ in both compounds. This observation indicates that despite the significant difference in donor ligand to metal electronic coupling in ***e*-1a** and ***e*-1b**, there is little difference in the rate of back ET in the two compounds. The significance of this finding with respect to the mechanism of LLCT excited state decay via back ET is discussed.

Experimental Section

Solvents and chemicals used for synthesis were of reagent grade and used without purification unless noted. Silica gel (Merck, 230−400 mesh) and neutral alumina (Fisher, Brockman grade III) were used for chromatography. NMR spectra were run on either GE QE-300 MHz or Varian VXR-300 MHz spectrophotometers. Metal complexes **2**,[16] **3a**,[13a] and (bpy)-$Re^{I}(CO)_3(CF_3SO_3)$[13b] were prepared as described previously. All Re(I) complexes were isolated as PF_6^- salts.

***p*-(4-Pyridyl)-*N*,*N*-dimethylaniline (4).** Freshly distilled pyridine (16 g, 0.2 mol), benzoyl chloride (14 g, 0.1 mol), and Cu powder (0.5 g, 8 mmol) were combined in a 1-L three-necked flask which was fitted with a mechanical stirrer and a reflux condensor. The reaction mixture was purged with dry N_2 and then heated and stirred for 1 h over a steam bath. After this period the reaction mixture was cooled, whereupon *N*,*N*-dimethylaniline (12 g, 0.1 mol) was added. The resulting solution was again purged with N_2 gas and then heated over a steam bath for 4 h. During this period the reaction mixture gradually solidified. After the 4-h heating period, the mixture was cooled, whereupon 30 mL of concentrated HCl was added. The acidified reaction mixture was then subjected to steam distillation for a 4-h period. The reaction mixture was then made basic by the addition of NaOH (15 g, 0.38 mol) dissolved in 50 mL of H_2O. At this point the product precipitated as a light brown mass. The brown product was collected by suction filtration, dried, and then purified by repeated sublimation. The purified product was obtained as a pale yellow solid, yield 2 g (10%): 1H NMR (300 MHz, $CDCl_3$) δ 3.12 (s, 6H), 6.81 (d, 2H), 7.72 (d, 2H), 7.83 (d, 2H), 8.53 (d, 2H).

CHART 1

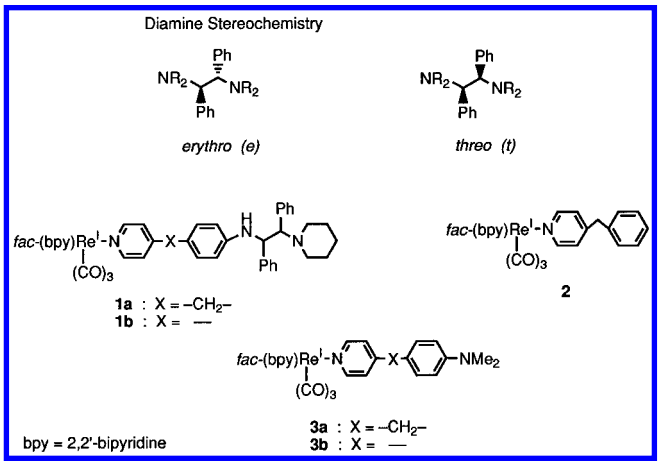

***erythro*-1-{*p*-[4-(Pyridyl)methyl]anilino}-2-piperidino)-1,2-diphenylethane (5).** A mixture of *erythro*-2-piperidino-1,2-diphenylethanol[17] (562 mg, 2.0 mmol), 10 mL of freshly distilled CH_2Cl_2, and triethylamine (0.8 mL, 6.0 mmol) was placed in a 100-mL three-necked round bottom flask, and the resulting solution was purged with N_2 for 30 min. During this period the temperature was adjusted to −20 °C by using a dry ice−2-propanol bath. A solution of methanesulfonyl chloride (0.155 mL, 2.0 mmol) dissolved in 2 mL of freshly distilled CH_2Cl_2 was added dropwise by using a syringe. The resulting mixture was maintained at −20 °C and stirred gently for 1 h. After this period of time a solution of *p*-[(4-pyridyl)methyl]aniline[13a] (370 mg, 2.0 mmol) in 3 mL of freshly distilled CH_2Cl_2 was added dropwise by using a syringe. After the temperature of the solution increased to ambient the solution was heated to reflux. During the reflux period the reaction was monitored by TLC (silica, ethyl acetate/hexane, 4:6 v/v). Refluxing was discontinued after 16 h, at which point *p*-[(4-pyridyl)methyl]-aniline was no longer visible by TLC. The solvent was removed under reduced pressure, and the crude product was purified by chromatography (silica, ethyl acetate/hexane, 4:6 v/v). Pure **5** was obtained as a yellow solid in 35% yield after purification: TLC (silica, ethyl acetate/hexane, 4:6 v/v) $R_f = 0.4$; ^{1}H NMR (300 MHz, $CDCl_3$) δ 1.45 (m, 2H), 1.56 (m, 4H), 2.45 (br, 4H), 3.45 (d, $J = 5.7$ Hz, 1H), 3.80 (s, 2H), 4.76 (d, $J = 5.7$ Hz, 1H), 5.0 (br, 1H), 6.45 (d, $J = 8.1$ Hz, 2H), 6.86 (d, $J = 8.1$ Hz), 6.9−7.25 (m, 12H), 8.45 (d, $J = 6.0$ Hz); ^{13}C NMR (75 MHz, $CDCl_3$) δ 24.6, 26.2, 40.4, 52.3, 58.9, 75.9, 114.4, 124.1, 126.5, 127.0, 127.3, 127.4, 127.5, 127.7, 129.1, 129.4, 137.6, 141.5, 146.7, 149.6, 150.8.

Complex *e*-1a. (All procedures described below were carried out in a dimly lighted room to minimize exposure of ***e*-1a** to light.) A mixture of (bpy)$Re(CO)_3$(TFMS) (115 mg, 0.2 mmol), **5** (134 mg, 0.3 mmol), NH_4PF_6 (326 mg, 2 mmol), and 5-mL of freshly distilled THF was stirred at 25 °C under a blanket of dry N_2 for 4 h. Excess NH_4PF_6 was removed by filtration, and

the THF solvent was removed under reduced pressure. The crude product was purified by chromatography on alumina eluting with CH_2Cl_2/CH_3CN (95:5 v/v). After removal of the chromatography solvent, the residue was dissolved in a minimal amount of CH_2Cl_2 and precipitated from *n*-pentane to produce a yellow powder, yield 102 mg (50%) after purification: TLC (silica, $CHCl_3$/MeOH, 96:4 v/v) $R_f = 0.2-0.3$; ^{1}H NMR (300 MHz, CD_3CN) δ 1.28 (br, 2H), 1.36 (br, 4H), 2.15 (br, 2H), 2.43 (br, 2H), 3.62 (d, $J = 8.1$ Hz, 1H), 3.67 (s, 2H), 4.8−4.9 (m, 2H, NH), 6.38 (d, $J = 8.1$ Hz, 2H), 6.72 (d, $J = 8.1$ Hz, 2H), 7.02 (d, $J = 6.3$ Hz, 2H), 7.1−7.3 (m, 10H), 7.75 (t, $J = 5.1$ Hz, 2H), 8.02 (d, $J = 6.3$ Hz, 2H), 8.24 (t, $J = 8.1$ Hz, 2H), 8.36 (d, $J = 8.1$ Hz, 2H), 9.16 (d, $J = 5.1$ Hz, 2H); ^{13}C NMR (75 MHz, CD_3CN) δ 24.1, 25.8, 39.1, 51.1, 57.4, 74.8, 124.4, 125.8, 126.2 (2C's), 126.7, 127.1, 127.2, 127.4, 128.5, 128.9, 129.2, 136.8, 140.8, 142.6, 146.5, 151.2, 153.5, 155.5, 156.0; HRMS (FAB, positive ion) calcd for $C_{44}H_{41}N_5O_3Re$, 874.277 (M^+); obsd, 874.273.

Complex *e*-1b. This complex was prepared according to the procedure described above for ***e*-1a**, except *erythro*-1-{*p*-[4-(pyridyl)]anilino}-2-piperidino-1,2-diphenylethane (**6a**)[17] was used in place of **5**. The crude product was purified by chromatography on alumina eluting with CH_2Cl_2/CH_3CN (9:1 v/v). After removal of the chromatography solvent, the residue was dissolved in a minimal amount of CH_2Cl_2 and precipitated from *n*-pentane to produce a yellow powder, yield 90 mg (45%) after purification: TLC (silica, CH_2Cl_2/CH_3CN 4:1 v/v) $R_f = 0.3-0.6$; ^{1}H NMR (300 MHz, CD_3CN) δ 1.25 (br, 2H), 1.33 (br, 4H), 2.15 (br, 2H), 2.46 (br, 2H), 3.70 (d, $J = 8.7$ Hz), 5.00 (m, 1H), 5.43 (br, 1H), 6.54 (d, $J = 8.7$ Hz, 2H), 7.1−7.4 (m, 14H), 7.77 (t, $J = 5.1$ Hz, 2H), 8.01 (d, $J = 6.3$ Hz, 2H), 8.24 (t, $J = 7.5$ Hz, 2H), 8.34 (d, $J = 7.5$ Hz, 2H), 9.20 (d, $J = 5.1$ Hz, 2H); ^{13}C NMR (75 MHz, CD_3CN) δ 24.2, 25.9, 51.2, 57.3, 74.8, 113.5, 121.5, 122.2, 124.5, 126.6, 127.0, 127.4, 127.6, 127.9, 128.6, 129.0, 136.5, 141.0, 142.1, 150.2, 150.6, 151.3, 153.6, 155.6; HRMS (FAB, positive ion) calcd for $C_{43}H_{39}N_5O_3Re$, 860.261 (M^+); obsd, 860.264.

[(bpy)Re(CO)$_3$(*p*-(4-pyridyl)-*N*,*N*-dimethylaniline)][PF$_6$] (3b). This complex was prepared according to the procedure described above for ***e*-1a**, except *p*-(4-pyridyl)-*N*,*N*-dimethylaniline (**4**) was used in place of **5**. The crude product was purified by chromatography on alumina eluting with CH_2Cl_2/CH_3CN (9:1 v/v). After removal of the chromatography solvent, the residue was dissolved in a minimal amount of CH_2Cl_2 and precipitated from *n*-pentane to produce a yellow powder, yield 125 mg (81%) after purification: TLC (silica, CH_2Cl_2/CH_3CN, 9:1 v/v) $R_f = 0.6-0.8$; ^{1}H NMR (300 MHz, CD_3CN) δ 2.97 (s, 6H), 6.72 (d, $J = 8.7$ Hz, 2H), 7.42 (d, $J = 6.3$ Hz, 2H), 7.55 (d, $J = 8.7$ Hz, 2H), 7.79 (t, $J = 5.1$ Hz, 2H), 8.05 (d, $J = 6.3$ Hz, 2H), 8.26 (t, $J = 8.1$ Hz, 2H), 8.37 (d, $J = 8.1$ Hz, 2H), 9.23 (d, $J = 5.1$ Hz, 2H); ^{13}C NMR (75 MHz, $CDCL_3$) δ 39.2, 112.2, 120.8, 121.4, 124.6, 127.9, 128.7, 141.0, 150.7, 151.4, 152.4, 153.7, 155.7; HRMS (FAB, positive ion) calcd for $C_{26}H_{22}N_4O_3Re$, 625.125 (M^+); obsd, 625.128.

[(bpy)Re(CO)$_3$(*p*-{4-(pyridyl)methyl}aniline)][PF$_6$] (7a). A mixture of (bpy)Re(CO)$_3$Cl (90 mg, 0.2 mmol), *p*-[(4-pyridyl)-methyl]aniline[13a] (74 mg, 0.4 mmol), and $AgPF_6$ (100 mg, 0.4 mmol) in 4 mL of DMF was heated to 80 °C for 3 h. After cooling, the solution was filtered through a medium-porosity fritted filter, and then the DMF was evaporated under reduced pressure. The residue was chromatographed on alumina using $CHCl_3$/MeOH (95:5 v/v) as eluant. After removal of the chromatography solvent, the residue was dissolved in a minimal amount of CH_2Cl_2 and precipitated from *n*-pentane to produce a yellow powder, yield 70 mg (50%) after purification: ^{1}H NMR (300 MHZ, CD_3CN) δ 3.76 (s, 2H), 6.53 (d, 2H), 6.82 (d, 2H), 7.08 (d, 2H), 7.77 (t, 2H), 8.06 (d, 2H), 8.27 (t, 2H), 8.38 (d, 2H), 9.19 (d, 2H).

***e*-1a Photoproduct Isolation and Characterization.** A solution of ***e*-1a** in CH_3CN (50 mg in 50 mL, $c = 0.7$ mM) was placed in a Pyrex test tube and degassed by bubbling with a stream of argon for 2 h. The resulting degassed solution was irradiated with a 450-W medium-pressure Hanovia mercury arc lamp for 80 min. The 366-nm emission of the Hg arc was isolated by using Corning 7−54 and Schott LG 350 glass filters. The photolyzed solution was concentrated and the residue was chromatographed on alumina using CH_2Cl_2/CH_3CN (95:5 v/v) as eluant. The fractions that contained the predominant yellow band from the column were combined, and the solvent was evaporated. The residue was dissolved in a minimal volume of CH_2Cl_2 and then precipitated by addition to *n*-pentane to yield 5 mg of a bright yellow powder: ^{1}H NMR (300 MHz, CD_3CN) δ 1.30 (m, 2H), 1.50 (m, 2H), 1.60 (m, 2H), 2.3 (m, the integral is obscured by a nearby H_2O resonance), 3.66 (1H, coupling obscured by nearby singlet), 3.71 (s, 2H), 4.62 (d, $J \approx 10.5$ Hz, 1H), 6.07 (1H), 6.48 (d, 2H), 6.77 (d, $J = 8.1$ Hz), 7.0−7.3 (m, 12H), 7.74 (t, 2H), 8.03 (d, $J = 5.1$ Hz), 8.24 (t, 2H), 8.35 (d, $J = 8.1$ Hz), 9.17 (d, 2H); ^{13}C NMR (75 MHz, CD_3CN) δ 24.0, 26.0, 39.1, 49.3, 57.4, 75.1, 124.3, 126.2, 126.4, 127.1, 127.2, 127.6, 127.8, 128.4, 129.2, 129.6, 133.4, 140.7, 142.8, 147.4, 151.2, 153.5, 155.5, 156.0; FAB-HRMS calcd for $C_{44}H_{41}N_5O_3Re$ (M^+) 874.277, found 874.284. The NMR and mass analysis are consistent with structure ***t*-1a**.

Procedures for Quantitative Photolyses. Quantum yield studies were carried out using equipment and procedures that have been described in detail in previous publications.[13a] HPLC analysis were carried out using a Whatman ODS-3 reversed phase column with a mobile phase consisting of THF/CH_3CN/H_2O (5:45:50 v/v/v) with 40 mM sodium heptane sulfonate and 50 mM triethylamine. All analyses were conducted with a detector wavelength of 250 nm.

As an example, the following is the procedure used for quantum efficiency measurements on ***e*-1a**. A 2-mL aliquot of an argon-degassed CH_3CN solution containing ***e*-1a** ($c = 0.5$ mM) was irradiated for 3 min (366 nm, 75-W high-pressure Hg lamp). Following light exposure, 0.5 mL of an internal standard solution (2 mM benzophenone in CH_3CN/H_2O, 9:1 v/v, pH = 3) was added to 2 mL of the photoproduct solution, and the mixture was analyzed by triplicate HPLC analysis.

For determination of quantum yields for ***e*-1a** → ***t*-1a** and ***e*-1b** → ***t*-1b** isomerization, it was assumed that the molar absorptivity of the *threo* and *erythro* isomers is the same at 250 nm.

Methods for Emission, Transient Absorption, and Electrochemical Experiments. Time-resolved emission, transient absorption, steady state emission, and electrochemistry were carried out by using methods and equipment that has been described in previous publications.[18] All transient absorption experiments were carried out by using a recirculating cell with a 100-mL volume to minimize the effects of sample decomposition during data acquisition.

Results

Structures. The structures of the Re(I) complexes discussed herein are illustrated in Chart 1. Complexes ***e*-1a,b** are the focus of the present study. These compounds contain the *fac*-(bpy)-Re(CO)$_3$-chromophore covalently linked to a 1,2-diamine "reactive donor". In ***e*-1a,b** the 1,2-diamine ligands are comprised of a 2° aromatic amine and a 3° aliphatic amine, and the diamine unit has *erythro* stereochemistry. The distinction between these

two complexes lies in the linkage between the pyridyl ligand and the aromatic amine portion of the diamine: in ***e*-1a** there is a methylene spacer, while in ***e*-1b** the methylene is absent, and therefore the aromatic amine and the pyridine are conjugated. This difference is significant, since conjugation in ***e*-1b** provides a pathway for strong electronic coupling between the aniline donor and the Re(I) center. The aniline to Re coupling is anticipated to be comparatively much weaker in ***e*-1a** due to the methylene spacer.

Complex **2** was studied to provide information concerning the dπ (Re) $\rightarrow$ π^* (bpy) MLCT excited state of the (bpy)-Re(CO)$_3$-chromophore, while complexes **3a,b** were examined to provide information concerning the effect of the aniline donor on the MLCT state without the complications associated with the diamine reactive donor. It is also important to note that a recent detailed report was published that examined the photophysical and photochemical properties of ligand **6a** (Chart 2).[17]

Photophysics. The absorption spectra of ***e*-1a,b**, **2**, **3a,b**, and **6a** were determined in CH_3CN. Table 1 contains a listing of absorption maxima and molar extinction coefficients, and Figure 1 illustrates the spectra of several representative complexes. The spectrum of **2** (Figure 1a), which illustrates the spectral features of the (bpy)Re(CO)$_3$-chromophore, is characterized by a moderately intense band with $\lambda_{max} \approx 350$ nm that is due to the dπ (Re) $\rightarrow$ π^* (bpy) MLCT absorption.[19] This complex also displays bands at 320 and 308 nm, which are assigned to π,π^* (bpy) intraligand transitions, while the intense features below 300 nm are a composite of π,π^* intraligand and MLCT transitions. The absorption of diamine complex ***e*-1a** is very similar to that of **2** at wavelengths longer than 300 nm (Figure 1a), except for a slightly increased absorptivity, which is likely due to weak n,π^* absorption of the aniline moiety in the diamine ligand.[13a] Complex ***e*-1a** also exhibits a strong band at $\lambda_{max} \approx$ 254 nm, which is attributed to the π,π^* transition of the aniline moiety.

The absorption spectrum of ***e*-1b** (Figure 1b) is distinct from that of model **2** or diamine ***e*-1a**. The most prominent feature in the absorption of ***e*-1b** is a band at $\lambda_{max} \approx 370$ nm that is considerably more intense than the near-UV MLCT absorption observed in ***e*-1a** and **2**. Comparison of the absorption of ***e*-1b** with that of diamine ligand **6a** (Figure 6b) indicates that the 370-nm absorption in the metal complex is likely due primarily to the intraligand π,π^* charge transfer (IL-CT) transition of the conjugated pyridyl−aniline chromophore. It is likely that there also is some contribution to the near-UV band from an underlying dπ (Re) $\rightarrow$ π^* (bpy) MLCT transition. Interestingly, the IL-CT transition of the pyridyl−aniline chromophore is significantly red-shifted and more intense in ***e*-1b** than in free ligand **6a**, which indicates that there is substantial electronic interaction between the aniline donor and the (bpy)Re(CO)$_3$-chromophore in the metal complex.

The luminescence properties of ***e*-1a,b**, **3a,b**, and **6a** were examined in degassed CH_3CN solution, and the results are also summarized in Table 1. Complex **2** exhibits a moderately intense and long-lived yellow luminescence which is typical of the (bpy)Re^{I}(CO)$_3$-chromophore and is attributed to the dπ (Re) $\rightarrow$ π^* (bpy) ^{3}MLCT excited state.[19] By contrast, each of the electron donor-substituted complexes ***e*-1a,b** and **3a,b** are virtually nonluminescent. Studies carried out with steady state and time-resolved photon counting indicate that in each case the upper limit for the ^{3}MLCT emission quantum yield and lifetime is 10^{-4} and 0.5 ns, respectively. This observation indicates that a nonradiative decay process is operative in the electron donor-substituted complexes, which accelerates the decay of the ^{3}MLCT state by greater than 10^2 relative to the decay rate in model complex **2**. The nonradiative decay pathway is attributed to forward ET from the donor ligand to the photoexcited Re center (k_{FET} path, Scheme 3).

CHART 2

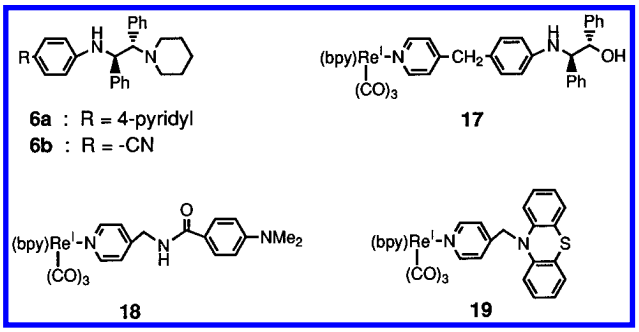

Photochemistry of Diamine-Substituted Complexes. Detailed studies were carried out to identify the products formed by irradiation of ***e*-1a** in air-saturated and argon-degassed CH_3CN solution. In both cases irradiation was effected using 366-nm light, which corresponds to the dπ (Re) $\rightarrow$ π^* (bpy) MLCT absorption. Scheme 2 provides a summary of the outcome of the photochemical reactions, and Table 2 provides a listing of the pertinent quantum efficiencies. Typical HPLC chromatograms for samples of ***e*-1a** which were irradiated to approximately 10% conversion are available as supporting information.

Photolysis of ***e*-1a** in air-saturated solution leads quantitatively to formation of pyridyl−aniline complex **7a** and benzaldehyde. These products were identified by comparison of HPLC retention times for peaks in the photoproduct solution with HPLC retention times of authentic samples of the two compounds. Benzeldehyde and **7a** are believed to form by photoinduced oxidative C−C bond fragmentation of the 1,2-diamine ligand in ***e*-1a**, followed by hydrolysis of the resulting imine complex **14a** and iminium ion **11** (Scheme 3). Quantum efficiency studies reveal that **7a** and benzaldehyde are formed in 1:1 and 2:1 ratios, respectively, relative to disappearence of ***e*-1a**, as expected on the basis of the reaction stoichiometry (Table 2). The quantum yield studies indicate that disappearence of ***e*-1a** under air-saturated conditions is quite efficient, with $\Phi = 0.54$.

The reaction mixture obtained by photolysis of ***e*-1a** in argon-degassed solution is more complicated. HPLC analysis of the argon-degassed reaction mixture indicates that, in addition to benzaldehyde and **7a**, another product is formed which has a slightly longer retention time than that of ***e*-1a** (see supporting information). Semipreparative photolysis of ***e*-1a** followed by silica gel chromatography afforded a small amount of the unknown material. Analysis by ^{1}H NMR, ^{13}C NMR, and high-resolution mass spectroscopy indicates that the additional product is the *threo* diastereomer, ***t*-1a** (see the Experimental Section). The *threo* diastereomer is likely formed by stereorandom recombination of the metal complex radical **10a** and ion **11**, which are formed by photoinduced oxidative C−C bond fragmentation of the 1,2-diamine ligand (Scheme 3).[15] Quantum efficiency studies indicate that the disappearance of ***e*-1a** is suppressed significantly in argon-degassed solution (Table 2). Fragmentation products **7a** and benzaldehyde are still formed in the expected 1:1 and 2:1 stoichiometry relative to disappearence of ***e*-1a**; however, under argon-degassed conditions the predominant reaction pathway becomes ***e*-1a** $\rightarrow$ ***t*-1a** photoisomerization. The suppressed quantum efficiency for disappearence of ***e*-1** under argon-degassed conditions is likely due to the fact that there is a significant fraction of bond

TABLE 1: Photophysical Data[a]

	absorption		emission		
complex	λ_{max}/nm ($\epsilon_{max}/10^3$ M^{-1} cm^{-1})	assignment	λ_{max}/nm	Φ_{em}	τ_{em}/ns
***e*-1a**	254 (38.5)	π,π^* IL (aniline)	*b*	$<10^{-4}$ [b]	<0.5[b]
	308 (17.8)	π,π^* bpy			
	320 (17.2)	π,π^* bpy			
	350 (5.3)	Re → bpy MLCT			
***e*-1b**	242 (29.9)	π,π^* IL	*b*	$<10^{-4}$ [b]	<0.5[b]
	312 (15.9)	π,π^* bpy			
	320 (18.8)	π,π^* bpy			
	370 (40.1)	IL CT & Re → bpy MLCT			
2	250 (20.0)	π,π^* IL	595	4.5×10^{-2}	210
	266 (19.4)	π,π^* IL			
	306 (11.9)	π,π^* bpy			
	320 (12.4)	π,π^* bpy			
	350 (3.7)	Re → bpy MLCT			
3a	262 (29.8)	π,π^* IL (aniline)	*b*	$<10^{-4}$ [b]	<0.5[b]
	308 (14.4)	π,π^* bpy			
	320 (12.8)	π,π^* bpy			
	350 (4.6)	Re → bpy MLCT			
3b	244 (28.1)	π,π^* IL	*b*	$<10^{-4}$ [b]	<0.5[b]
	310 (14.4)	π,π^* bpy			
	320 (16.5)	π,π^* bpy			
	382 (40.0)	IL CT & Re → bpy MLCT			
6a	318 (25.0)	π,π^* CT	392		1.1

[a] All data in degassed CH_3CN solution at 25 °C. [b] Emission too weak for accurate determination.

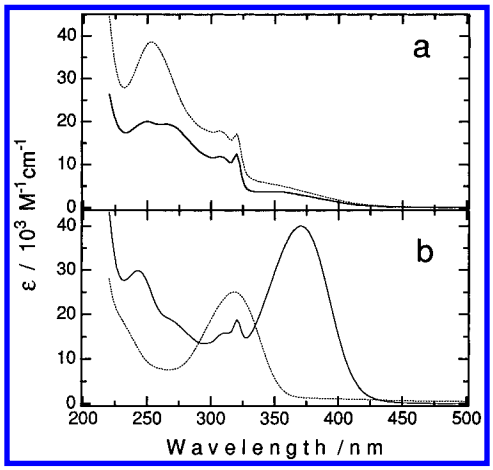

Figure 1. UV−visible absorption spectra of CH_3CN solutions: (a) solid line, **2**; broken line, ***e*-1a**; (b) solid line, ***e*-1b**; broken line, **6a**.

fragmentation events which are unproductive due to recombination to form the starting complex ***e*-1a**.[17]

Steady state photochemical studies of ***e*-1b** were also effected by using 366-nm photolysis, which excites largely the IL-CT transition of the pyridyl−aniline chromphore of the diamine ligand. However, despite this feature, the product distribution and overall quantum efficiency of the photochemistry of ***e*-1b** is remarkably similar to that of ***e*-1a** (see Scheme 2 and Table 2). Irradiation of ***e*-1b** in air-saturated CH_3CN solution leads to exclusive formation of benzaldehyde and pyridyl−aniline complex **7b**, which were identified by comparison of HPLC retention times for peaks in the photoproduct solution with HPLC retention times of authentic samples of the two compounds. Benzaldehyde and **7b** presumably form via a pathway analogous to that described for fragmentation of the diamine ligand in ***e*-1a** (Scheme 3). Quantum yield studies indicate that benzaldehyde is formed in approximately 2:1 stoichiometry relative to disappearence of ***e*-1b**, as anticipated on the basis of the reaction stoichiometry. The overall quantum efficiency for disappearence of ***e*-1b** under air-saturated conditions is slightly lower compared to that of ***e*-1a**, but the reaction remains comparatively efficient with $\Phi^- = 0.43$.

As for complex ***e*-1a**, irradiation of ***e*-1b** in argon-degassed CH_3CN leads to a more complex reaction mixture. Benzaldehyde and **7b** are still formed under argon-degassed conditions; however, a new compound with a slightly longer HPLC retention time compared to that of ***e*-1b** is detected. Although this compound was not isolated and identified by semipreparative irradiation, the close similarity of the HPLC chromatograms for the ***e*-1a** and ***e*-1b** air-saturated photoproduct solutions strongly implies that the unidentified peak at longer retention time is the *threo* diastereomer, ***t*-1b**. Quantum yield studies indicate that the efficiency for disappearance of ***e*-1b** is suppressed under argon-degassed conditions and that the dominant reaction pathway appears to be ***e*-1b** → ***t*-1b** photoisomerization (Table 2).

Transient Absorption Spectroscopy. Nanosecond−microsecond laser flash photolysis studies were carried out on ***e*-1a,b** and **3a,b** to examine the spectroscopic properties and dynamics of the excited states and reactive intermediates involved in the photochemistry and photophysics of these complexes. Picosecond pump−probe studies were also carried out on ***e*-1a** and **3a**, and the findings of this work are described elsewhere.[13c] All nanosecond−microsecond laser flash photolysis studies were carried out by using the third harmonic of a Nd:YAG laser for excitation (355 nm, 10 ns fwhm, 10 mJ/pulse). Listed delay times correspond to delay after the leading edge of the laser excitation pulse.

Figure 2a illustrates the transient absorption spectrum of **3a** obtained at 10-ns delay following the leading edge of the laser pulse. This spectrum is characterized by a comparatively weak, broad absorption centered at $\lambda_{max} = 490$ nm ($\Delta A_{max} = 0.078$). The transient absorption decays too rapidly for accurate determination of the decay rate with the nanosecond apparatus (see inset to Figure 2a); however, picosecond pump−probe spectroscopy indicates that the decay rate of this transient is 1×10^8 s^{-1}.[13c] The transient absorption spectrum of **3a** is substantially different from that of the dπ (Re) → π^* (bpy) MLCT excited state in model complex **2**, which displays a strong, narrow absorption band with $\lambda_{max} \approx 370$ nm.[20] On this basis, the transient absorption spectrum of **3a** is attributed to LLCT excited state **16a** (eq 3), which is formed by a sequence that involves initial excitation to the MLCT state **15a**, followed by

SCHEME 2

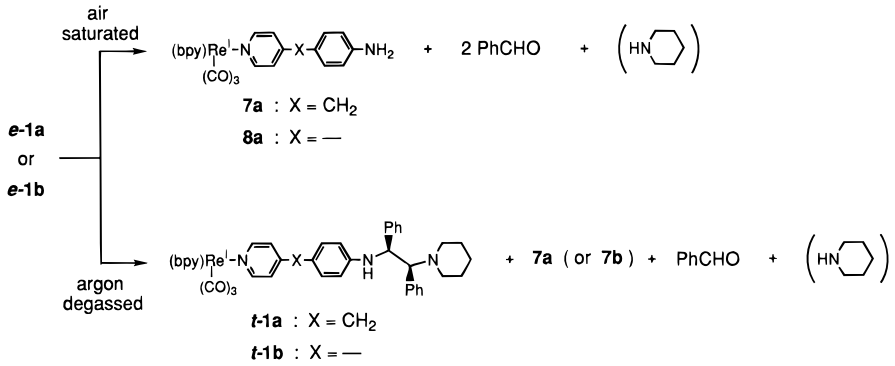

TABLE 2: Photochemical Quantum Efficiencies[a]

	air saturated				argon degassed			
complex	Φ^-	Φ_{threo}	Φ_{PhCHO}	Φ_{amine}	Φ^-	Φ_{threo}	Φ_{PhCHO}	Φ_{amine}
***e*-1a**	0.54 ± 0.03	<0.01	1.10 ± 0.05	0.48 ± 0.01	0.29 ± 0.04	0.16 ± 0.01	0.19 ± 0.02	0.08 ± 0.01
***e*-1b**	0.43 ± 0.02	<0.01	0.75 ± 0.04	*b*	0.26 ± 0.03	0.09 ± 0.02	0.14 ± 0.02	*b*

[a] All data for CH_3CN solutions at 25 °C. Φ^-, quantum yield for disappearence of starting complex; Φ_{threo}, quantum yield for *erythro* → *threo* photoisomerization; Φ_{PhCHO}, quantum yield for benzaldehyde formation; Φ_{amine}, quantum yield for formation of **7a** or **7b**. [b] Not determined.

SCHEME 3

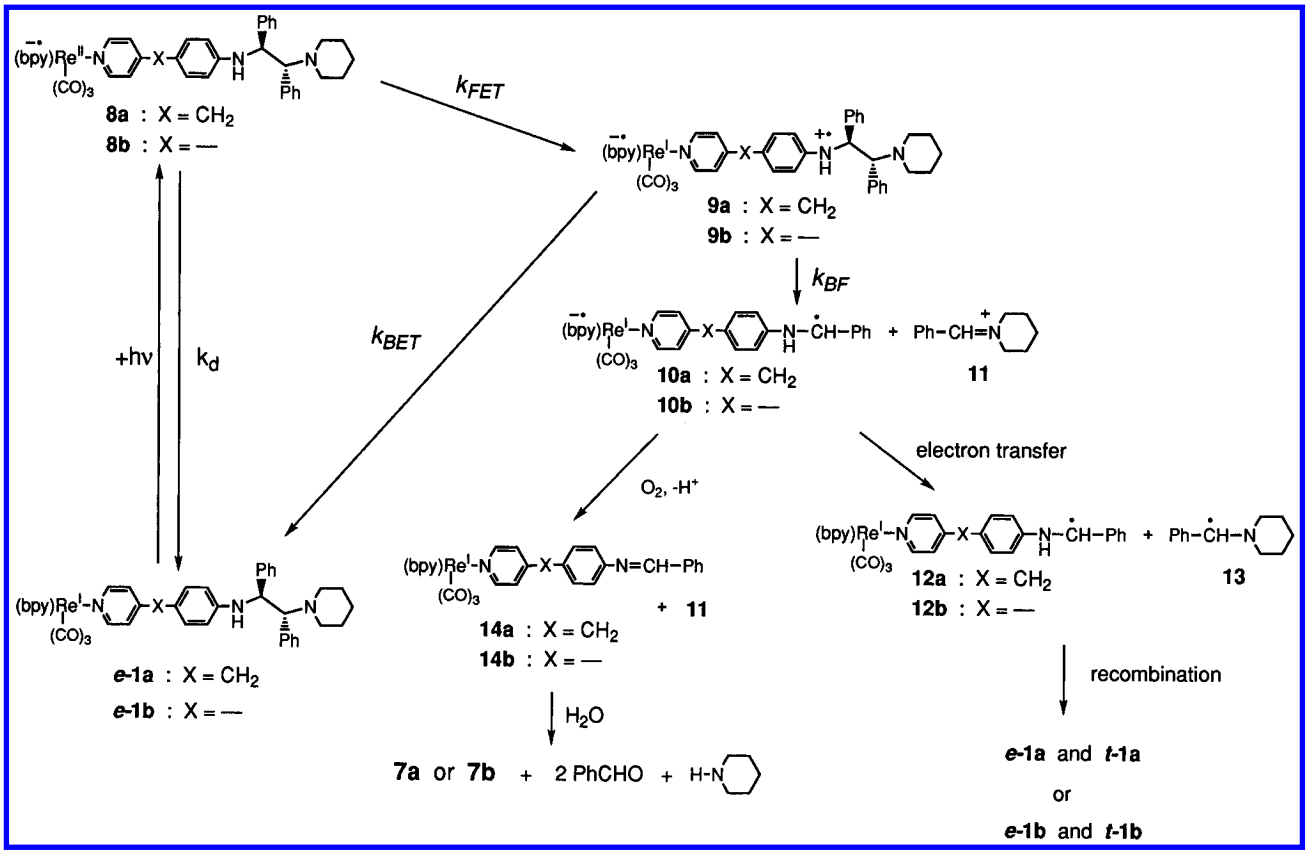

rapid forward ET ($k_{FET} \gg 10^9\ s^{-1}$). An important point for the present study is that the picosecond measurement of the decay rate of LLCT state **16a** indicates that the rate of back ET in this aniline-substituted complex is $k_{BET} = 1 \times 10^8\ s^{-1}$.[13c]

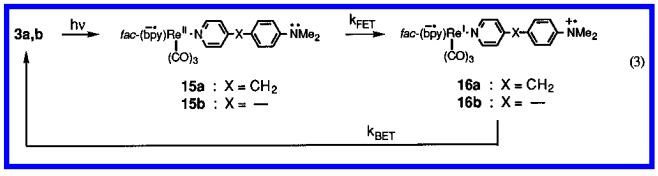

Nanosecond transient absorption spectroscopy was carried out on pyridyl−aniline complex **3b**, and the spectroscopic and kinetic findings are summarized in Figure 2b. The transient absorption of this complex is dominated by a moderately strong bleach at $\lambda_{max} \approx 390$ nm and weak aborption in the mid-visible. The bleach at 390 nm corresponds to the ground state absorption band that is assigned to the π,π^* IL-CT absorption of the pyridyl−aniline donor ligand. Two observations suggest that the transient absorption spectrum observed for **3b** is due to the LLCT state **16b**, eq 3. First, the spectrum differs significantly from that of the dπ (Re) → π^* (bpy) MLCT state.[20] Second, the strong bleach of the IL-CT absorption band indicates that there is depletion of electron density at the aniline donor in the transient, which is consistent with the electronic structure of

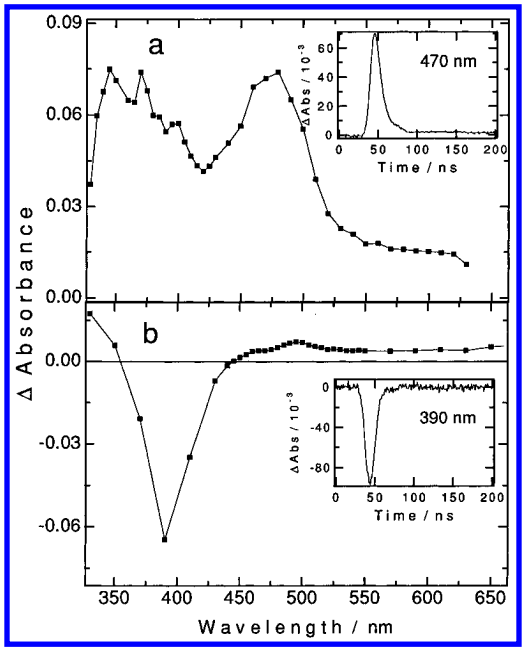

Figure 2. Transient absorption difference spectra following laser excitation (355 nm, 10 ns fwhm, 10 mJ/pulse). All spectra are for degassed CH_3CN solutions. Delays refer to delay time from leading edge of laser excitation pulse. (a) **3a**, 10 ns delay. Inset: transient absorption kinetics of **3a** at 470 nm. (b) **3b**, 10 ns delay. Inset: transient absorption kinetics of **3b** at 390 nm.

LLCT state **16b**. The transient absorption of **3b** decays too rapidly for accurate determination by using the nanosecond system (see inset to Figure 2b); however, the fact that a moderately strong transient absorption is observed with nanosecond laser excitation implies that the decay rate of the transient is $\leq 10^9$ s^{-1}.

Figure 3 provides a summary of the transient absorption data for ***e*-1a** in degassed CH_3CN solution. Parts a and b of Figure 3 illustrate spectra at delay times ranging from 5 to 1000 ns and 5 to 325 μs, respectively, while the insets to parts a and b of Figure 3 illustrate the temporal profile of the transient absorption at 460 and 365 nm, respectively. Taken together, these data clearly indicate that near-UV excitation of ***e*-1a** leads to rapid formation of a strongly absorbing transient with $\lambda_{max} \approx 360$ nm. For reasons that will be fully outlined below, this transient absorption spectrum is assigned to metal complex radical **10a** (Scheme 3) that is produced by C−C bond fragmentation of the diamine ligand in ***e*-1a**. The 360-nm transient is formed almost completely during the laser pulse; however, the early time transient absorption data (refer to Figure 3a) imply that there is a spectral evolution that occurs which is slightly too fast to be temporally resolved by the nanosecond system. Recently published picosecond transient absorption studies of ***e*-1a** allow resolution of these fast dynamics and indicate that the rise time of the 360-nm absorption and the fast decay of the absorption at 460 nm (see inset, Figure 3a) occur with the same first-order rate of $k = 4 \times 10^8$ s^{-1}.[13c]

The microsecond time domain data shown in Figure 3b indicate that the 360-nm transient attributed to metal complex radical **10a** decays comparatively slowly. Kinetic analysis reveals that the decay can be modeled by assuming second-order, equal concentration kinetics. A fit of the data provides $k_2/\Delta\epsilon = 3.0 \times 10^4$ cm s^{-1}, where k_2 is the second-order decay rate constant (units = M^{-1} s^{-1}) and $\Delta\epsilon$ is the difference molar absorptivity (units = M^{-1} cm^{-1}) of the transient absorption at 360 nm. Assuming that $\Delta\epsilon \approx 2 \times 10^4$ M^{-1} cm^{-1} leads to an estimate of $k_2 \approx 6 \times 10^8$ M^{-1} s^{-1}.

Figure 4 provides a summary of the transient absorption data

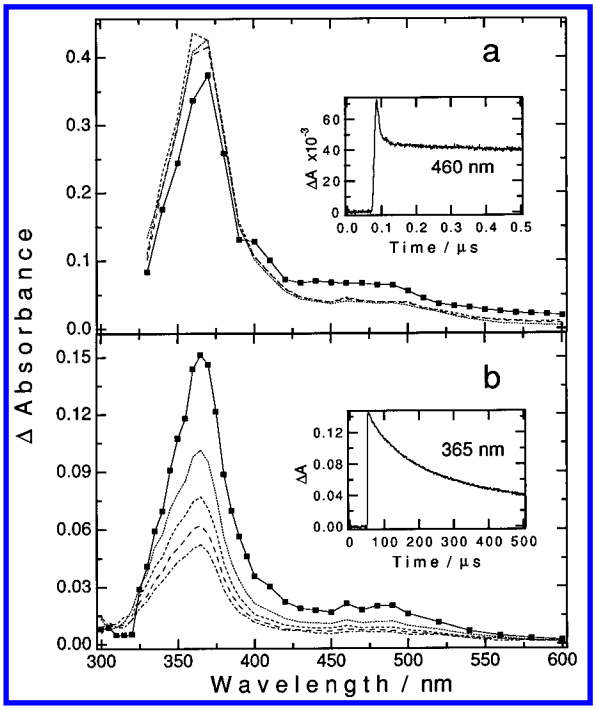

Figure 3. Transient absorption difference spectra of ***e*-1a** in degassed CH_3CN following laser excitation (355 nm, 10 ns fwhm, 10 mJ/pulse). Delays refer to delay time from leading edge of laser excitation pulse. (a) Delay times: 5 ns (−■−), 100 ns (− −), 200 ns (···), and 1000 ns (- - -). INSET: transient absorption kinetics at 460 nm. (b) Delay times (in order of decreasing transient absorption intensity): 5, 50, 100, 200, 250, and 325 μs. INSET: transient absorption kinetics at 365 nm.

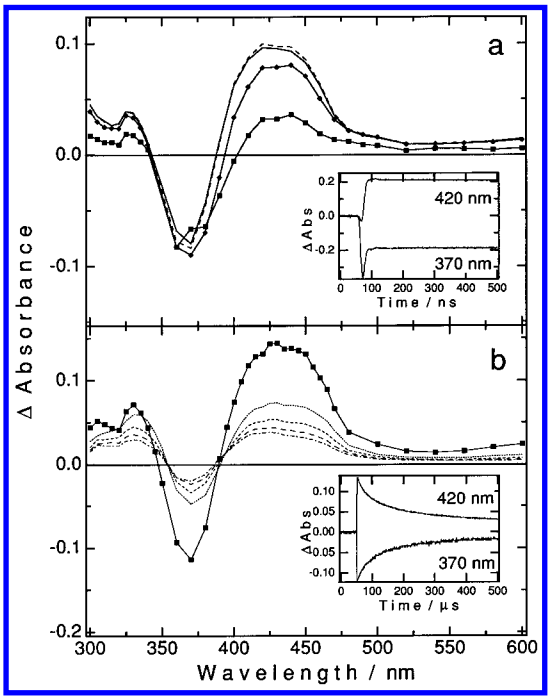

Figure 4. Transient absorption difference spectra of ***e*-1b** in degassed CH_3CN solution following laser excitation (355 nm, 10 ns fwhm, 10 mJ/pulse). Delays refer to delay time from leading edge of laser excitation pulse. (a) Delay times (in order of increasing transient absorption intensity at 425 nm): 10, 30, 50, and 100 ns. Inset: transient absorption kinetics at 370 and 420 nm. (b) Delay times (in order of decreasing transient absorption intensity at 425 nm): 5, 50, 100, 200, 250, and 325 μs. Inset: transient absorption kinetics at 370 and 420 nm.

for ***e*-1b** in degassed CH_3CN solution. Parts a and b of Figure 4 illustrate spectra at delay times ranging from 5 to 100 ns and

5 to 325 μs, respectively, while the insets to parts a and b of Figure 4 illustrate the temporal profile of the transient absorption at 420 and 370 nm, respectively. The transient absorption spectra clearly indicate that photoexcitation of ***e*-1b** leads very rapidly to (1) significant bleaching of the ground state absorption band at 370 nm, which is due to the IL-CT absorption of the pyridyl−aniline chromophore, and (2) production of a strongly absorbing transient with an apparent absorption maximum at $\lambda \approx 425$ nm. For reasons that will be fully explained in the Discussion section, the transient absorption features observed for ***e*-1b** are ascribed to photoinduced fragmentation of the diamine ligand and production of metal complex radical **10b** (Scheme 3). Bleaching of the ground state absorption at 370 nm is due to loss of the IL-CT absorption of the pyridyl−aniline chromophore, while the transient absorption feature at 425 nm is assigned to **10b**. While the photoinduced fragmentation is very fast on the nanosecond time scale, the early time data (Figure 4a) indicate that there is a dynamic process which occurs during and immediately following the 10-ns laser pulse. Significantly, the spectrum at the earliest delay time (10-ns delay) exhibits a fully developed bleach at 370 nm. By contrast, the 425-nm transient absorption rises comparatively more slowly, taking ≈30 ns to fully develop. These features suggest that bond fragmentation (e.g., **9b** → **10b**) occurs on a time scale that is very close to the temporal resolution of the nanosecond flash photolysis system (e.g., $k_{BF} < 10^9$ s^{-1}).

The microsecond time domain transient absorption data for ***e*-1b** (Figure 4b) reveal that the transient absorption and bleach signals that are attributed, respectively, to **10b** and depletion of ***e*-1b** decay within approximately 500 μs of the pulse. Interestingly, a substantial fraction of the ground state bleaching in the near-UV region recovers, which is consistent with recombination of the radicals formed by bond fragmentation to regenerate the starting complex. The transient absorption and bleach recovery kinetics can be modeled by assuming second-order, equal concentration kinetics. A fit of the transient absorption kinetic data at 420 nm provides $k_2/\Delta\epsilon = 2.0 \times 10^5$ cm s^{-1}. Assuming that $\Delta\epsilon_{420} \approx 2 \times 10^4$ M^{-1} cm^{-1} leads to $k_2 \approx 4 \times 10^9$ M^{-1} s^{-1} for recovery of the bleach signal.

Nanosecond transient absorption studies carried out on ***e*-1a** and ***e*-1b** in air-saturated CH_3CN solution indicate that under these conditions metal complex radicals **10a** and **10b** are formed by laser excitation. However, in the presence of O_2 these transients are quenched exceedingly rapidly, with $k \approx 1 \times 10^7$ s^{-1}. Assuming that $[O_2] \approx 1.9$ mM in air-saturated CH_3CN solution, the second-order rate constant for reaction of these radicals with O_2 is $\approx 5 \times 10^9$ M^{-1} s^{-1}, which is close to the diffusion-controlled limit in CH_3CN.

Electrochemistry and Thermodynamics for Intramolecular ET. Cyclic voltammetry was carried out on ***e*-1a,b**, **2**, **3a**, and various model amines to determine (1) the potentials for oxidation of the diamine (or amine) donor ligand and for reduction of the bpy acceptor ligand and (2) to attempt to identify the site at which oxidation occurs within the diamine unit. Table 3 lists the electrochemical potentials for these compounds relative to the saturated sodium chloride calomel electrode (SSCE). First, cathodic scans for each of the metal complexes reveal a reversible wave at $E_{1/2} \approx -1.17$ V. In each case this wave is ascribed to reduction of the coordinated bpy ligand.[19] Anodic scans for the two diamine complexes ***e*-1a** and ***e*-1b** and the dimethylaniline-substituted complex **3a** display an irreversible wave each, with $E_p \approx +0.85$ V. This wave is not observed in model complex **2** (which does not contain an amine donor ligand), and on this basis it is attributed to oxidation of the aniline or diamine donor. Table 3 also contains a listing of peak potentials for irreversible oxidation of *N*-benzylpiperidine, *N*-methylaniline, and *N*,*N*-dimethylaniline.[21] This data reveals that the irreversible oxidation of *N*-benzylpiperidine (a 3° aliphatic amine) is shifted several hundred millivolts anodic compared to the oxidation of *N*-methylaniline and *N*,*N*-dimethylaniline (typical aromatic amines).

TABLE 3: Electrochemical Potentials[a]

compound	E_p^{ox}/V[b]	$E_{1/2}^{red}$/V[c]	ΔG_{FET}/eV	ΔG_{BET}/eV
***e*-1a**	+0.84	−1.17	−0.37	−2.01
***e*-1b**	+0.85	−1.17	−0.36	−2.02
2		−1.16		
3a	+0.82[f]	−1.17	−0.39	−1.99
N-benzylpiperidine	+0.97			
N-methylaniline	+0.72[g]			
N,*N*-dimethylaniline	+0.77[g]			

[a] All potentials for CH_3CN solutions with 0.1 M TBAH supporting electrolyte. Potentials relative to saturated sodium chloride calomel reference electrode. [b] Peak potential for irreversible anodic wave at 100 mV/s sweep rate. [c] Half-wave potential for reversible cathodic wave. [d] Free energy change for photoinduced forward electron transfer. [e] Free energy change for back electron transfer. [f] Half-wave potential for quasi-reversible anodic wave. [g] Potentials from ref 30.

All of the available information suggests that the oxidation of the diamine ligands in ***e*-1a,b** is localized primarily at the aniline unit (and not at the piperidine site). First, the peak anodic potentials of ***e*-1a,b** occur at approximately the same potential as the quasi-reversible oxidation of the *N*,*N*-dimethylaniline unit in **3a**. Note that the peak anodic potentials for ***e*-1a,b** and **3a** are slightly more positive than the oxidation potentials of *N*-methylaniline or *N*,*N*-dimethylaniline; however, the positive shift of the aniline-based oxidation in the metal complexes is likely due to a net +1 charge on the complexes. Despite the slight positive shift, the anodic waves for ***e*-1a** and ***e*-1b** still occur at a less positive potential compared to oxidation of the piperidine model compound *N*-benzylpiperidine, which further substantiates the view that the oxidation in the diamine complexes occurs at the aniline donor unit.

The free energy change that accompanies photoinduced forward and back ET (ΔG_{FET} and ΔG_{BET}, respectively) in ***e*-1a,b** and **3a,b** can be estimated by the following expressions:[22]

$$\Delta G_{FET} \approx E_p(D/D^{\bullet+}) - E_{1/2}(bpy/bpy^{\bullet-}) - E_{00} \quad (4a)$$

$$\Delta G_{BET} \approx E_{1/2}(bpy/bpy^{\bullet-}) - E_p(D/D^{\bullet+}) \quad (4b)$$

where $E_p(D/D^{\bullet+})$ is the peak oxidation potential of the aniline or diamine donor ligand, $E_{1/2}(bpy/bpy^{\bullet-})$ is the half-wave reduction potential of the bpy acceptor ligand, and E_{00} is the 0−0 energy of the relaxed MLCT excited state of the (bpy)-$Re^I(CO)_3$-chromophore. By using the electrochemical potentials listed in Table 3 along with E_{00} estimated from the emission spectrum of **2** in CH_3CN ($E_{00} \approx 17\,550$ cm^{-1}),[16] ΔG_{FET} and ΔG_{BET} for each complex have been estimated, and the values are listed in Table 3. These calculations indicate that for each complex forward ET is moderately exothermic and back ET is strongly exothermic.

Discussion

Overall Mechanism for Photochemistry. Scheme 3 presents an overall mechanism that is consistent with the observed photochemical and photophysical properties of ***e*-1a,b**. Initial photoexcitation produces the relaxed dπ (Re) → π^* (bpy) MLCT excited state **8**.[23] The MLCT state relaxes via radiative and nonradiative decay to the ground state (k_d path) or by forward ET from the diamine donor to the photoexcited Re(I) center

(k_{FET} path). Forward ET produces LLCT state **9**. In a one-electron approximation, **9** comprises a bpy anion radical (e.g., $bpy^{\bullet -}$) and a diamine radical cation held in proximity by the transition metal center. LLCT state **9** relaxes either by back ET (k_{BET} path) via transfer of an electron from $bpy^{\bullet -}$ to the diamine radical cation or by C−C bond fragmentation of the diamine radical cation (k_{BF} path). Bond fragmentation within **9** occurs in a formally heterolytic fashion (*vide infra*) to produce metal complex radical **10** and iminium ion **11**, which is derived from the piperidine portion of the diamine unit. Under air-saturated conditions radical **10** is quenched by rapid ET to O_2,[13b] followed by loss of a proton to form imine complex **14**. Imine complex **14** and iminium ion **11** hydrolyze under HPLC analysis conditions to form the corresponding free amines (**7** and piperidine) and 2 equiv of benzaldehyde.

Under argon-degassed conditions, metal complex radical **10** survives for a sufficient period to allow it to react in a bimolecular reaction with iminium ion **11** in a two-step sequence that results in net regeneration of starting complex ***e*-1a** (or ***e*-1b**) and the corresponding diastereomer ***t*-1a** (or ***t*-1b**). The first step of this recombination sequence presumably involves ET from $bpy^{\bullet -}$ in **10** to iminium ion **11**, and the second step involves stereorandom recombination of **12** and **13** to produce the diastereomeric complexes ***e*-1** and ***t*-1** in approximately equivalent proportions.[17] The mechanism of this recombination reaction will be discussed in more detail in a succeeding section.

Kinetics of ET and Bond Fragmentation in *e*-1a and *e*-1b. The kinetics for forward ET in the donor-substituted complexes are given by the expression[22]

$$k_{FET} = 1/\tau - 1/\tau(\mathbf{2}) \qquad (5)$$

where τ and $\tau(\mathbf{2})$ are, respectively, the MLCT emission lifetimes of the donor-substituted complexes and model complex **2**. Emission lifetime studies indicate that the MLCT emission lifetimes of all of the donor-substituted complexes (e.g., ***e*-1a,b** and **3a,b**) are less than 0.5 ns (Table 1). Using eq 5 and the MLCT emission lifetime of model complex **2** (210 ns) leads to the conclusion that $k_{FET} \geq 2 \times 10^9\ s^{-1}$ in each of the donor-substituted complexes.

The rate of back ET (k_{BET}) was directly determined in model complex **3a** to be $1 \times 10^8\ s^{-1}$ by using picosecond transient absorption.[13c] While k_{BET} cannot be directly determined in diamine complex ***e*-1a**, it is reasonable to assume that **3a** serves as an excellent model for ***e*-1a** and, therefore, that $k_{BET} \approx 1.0 \times 10^8\ s^{-1}$ for ***e*-1a** as well. Further support for this conclusion comes from the fact that the rate of back ET is very similar in the structurally similar aminoalcohol complex **17** (Chart 2), where $k_{BET} = 8.3 \times 10^7\ s^{-1}$.[13a]

With a value for k_{BET} for ***e*-1a** in hand, it is possible to determine k_{BF} for ***e*-1a** from the picosecond transient absorption data. The kinetic model presented in Scheme 3 indicates that disappearance of **9a** and appearance of **10a** should occur with the same first-order rate constant, k_{obs}, where $k_{obs} = k_{BET} + k_{BF}$. Consistent with this premise, the picosecond transient absorption studies reveal that the decay of LLCT state **9a** and the grow-in of radical **10a** both occur with $k_{obs} = 4 \times 10^9\ s^{-1}$.[13c] Hence, the assumption that $k_{BET} = 1.0 \times 10^8\ s^{-1}$ affords a value of $k_{BF} = 3.0 \times 10^8\ s^{-1}$ for ***e*-1a**.

Picosecond transient absorption studies have not been carried out on ***e*-1b** or the relevant model complex **3b** to evaluate k_{BET} or k_{BF} in these complexes. However, by assuming that the rate of bond fragmentation is the same in the LLCT excited state of both ***e*-1a** and ***e*-1b** ($k_{BF} = 3.0 \times 10^8\ s^{-1}$),[24] it is possible to apply the steady state photochemical results on ***e*-1b** to provide an estimate for k_{BET} in this complex. By reference to Scheme 3, the overall efficiency for bond fragmentation (ϕ_{BF}) is given by the product of the efficiencies for formation of LLCT state **9b** by forward ET (ϕ_{LLCT}) and for formation of the radical **10b** by bond fragmentation (β_{BF}),[25]

$$\phi_{BF} = \phi_{LLCT}\beta_{BF} \qquad (6a)$$

where

$$\phi_{LLCT} = \frac{k_{FET}}{k_{FET} + k_d} \quad \text{and} \quad \beta_{BF} = \frac{k_{BF}}{k_{BF} + k_{BET}} \qquad (6b)$$

Transient absorption indicates that O_2 is an effective scavenger for radical **10b**, which is the primary product of bond fragmentation. Therefore, it is reasonable to assume that bond frgmentation is irreversible under air-saturated conditions and hence that $\phi_{BF} = \Phi_{-}^{air}$, where Φ_{-}^{air} is the quantum yield for disappearance for ***e*-1b** in air-saturated solution. Taking this into account, rearranging and combining eqs 6a and 6b leads to eq 7,

$$k_{BET} = k_{BF}(1 - \Phi_{-}^{air}) \qquad (7)$$

where it has also been assumed that $\phi_{BF} = \Phi_{-}^{air}$ and $\phi_{LLCT} = 1$. The latter assumption is justified by the fact that $k_{FET} \gg k_d$. Now, substituting $k_{BF} = 1.0 \times 10^8\ s^{-1}$ and $\Phi_{-}^{air} = 0.43$ into eq 7 leads to $k_{BET} \approx 1.3 \times 10^8\ s^{-1}$ for ***e*-1b**.

A summary of the rate constants for forward ET, back ET, and bond fragmentation in ***e*-1a**, ***e*-1b**, and **3a** is provided in Table 4. Several points merit discussion concerning these data. First, given that forward ET is moderately exothermic (≈−0.4 eV) and that the separation distance between the aniline donor and the Re(I) center is relatively small (ca. 5−7 Å), the fact that $k_{FET} \geq 2 \times 10^9\ s^{-1}$ is not unreasonable. Further, the rapid forward ET rates observed for ***e*-1a,b** and **3a** are consistent with the donor−acceptor electronic coupling matrix element (H_{AB}) and reorganization energy (λ) determined by a study of the temperature dependence for photoinduced forward ET in the structurally similar donor-substituted complex **18** (Chart 2), where $H_{AB} = 7\ cm^{-1}$ and $\lambda = 1.0$ eV.[12d]

TABLE 4: Electron Transfer and Bond Fragmentation Rates[a]

compound	k_{FET}/s^{-1}	k_{BET}/s^{-1}	k_{BF}/s^{-1}
***e*-1a**	$>2 \times 10^9$	1.0×10^8	3.0×10^8
***e*-1b**	$>2 \times 10^9$	1.3×10^8	3.0×10^8
3a	$>2 \times 10^9$	1.0×10^8	

[a] Data for CH_3CN solution. Rates estimated as described in text.

The rates for back ET in ***e*-1a,b** and **3** are comparable to values previously observed for strongly exothermic back ET in the related Re(I) complexes **18** ($k_{BET} = 1.3 \times 10^7\ s^{-1}$, $\Delta G_{BET} = -2.13$ eV)[13d] and **19** ($k_{BET} = 4.0 \times 10^7\ s^{-1}$, $\Delta G_{BET} = -1.96$ eV).[7b] However, despite the similarity among the rates for charge recombination in these structurally related Re(I) complexes, there are some surprising features. First, electronic coupling between the Re center and the aniline donor unit is likely to be significantly larger in ***e*-1b** than in ***e*-1a** because of the structural difference in the donor ligands for the two complexes.[26,27] Evidence of strong donor ligand−metal electronic coupling in ***e*-1b** is provided by the significant shift in the energy of the π,π^* IL-CT absorption of the pyridyl−aniline ligand in complex ***e*-1b** compared to the energy of the same transition in free ligand **6a**. However, despite the significant difference in donor ligand−metal coupling between ***e*-1a** and ***e*-1b**, k_{BET} is virtually the same within experimental error in the two complexes. Another surprise is that k_{BET} for the group

of donor-substituted complexes ***e*-1a,b**, **3a**, **18**, and **19** (and others) is comparatively slow compared to the rates of charge recombination in other donor−acceptor systems where the driving force and electronic coupling are comparable. For example, back ET in covalently linked porphyrin−quinone systems with donor−acceptor separation distances ranging from 5 to 10 Å and with $\Delta G_{BET} \approx 1.5$ eV typically occurs with $k_{BET} \approx 10^9-10^{10}$ s^{-1}.[28]

Taken together, the features outlined above imply that the rate of back ET in donor-substituted Re(I) complexes such as **1a,b**, **3a**, **18**, and **19** may be controlled, at least in part, by the dynamics of triplet → singlet intersystem crossing in the LLCT state. Intersystem crossing may play a role in determining the rate of back ET in the LLCT state because it is formed by forward ET from the MLCT state, which is believed to possess considerable triplet spin character (e.g., ^{3}MLCT → ^{3}LLCT).[29] Since the product of back ET (the ground state) has singlet spin multiplicity, intersystem crossing must precede decay of ^{3}LLCT via back ET.

That spin state dynamics play an important role in determining the lifetimes of charge-separated states formed by ET quenching in d^6 transition metal complex systems has been recently demonstrated by studies of heavy atom and magnetic field effects on ET reactions between ^{3}Ru(bpy)$_3^{2+}$* and electron donors or acceptors.[30] These studies indicate that the geminate radical pairs formed by oxidative or reductive ET quenching of ^{3}Ru(bpy)$_3^{2+}$* have a high degree of triplet spin character and, furthermore, that back ET in the geminate pairs is controlled largely by the dynamics of intersystem crossing.[30] Since spectroscopic studies indicate that the orbital and spin characteristics of the luminescent ^{3}MLCT excited states of Ru(bpy)$_3^{2+}$ and (bpy)Re(CO)$_3$L$^+$ complexes are virtually identical,[29] it is reasonable to expect that intersystem crossing dynamics will play an important role in photoinduced ET reactions in the (bpy)Re(CO)$_3$L$^+$ system as well.

Mechanism and Thermodynamics for Bond Fragmentation in the LLCT State. In Scheme 3, C−C bond fragmentation of the diamine radical cation within LLCT state **10** is implicitly considered to occur in a heterolytic mode. However, as illustrated by eq 8, fragmentation may occur in either a heterolytic or homolytic mode. These two bond fragmentation modes differ in outcome: heterolytic fragmentation (eq 8a) would produce metal complex **10** and piperidine iminium ion **11**, while homolytic fragmentation (eq 8b) would produce metal complex iminium ion **20** and piperidine α-amino radical **13**.

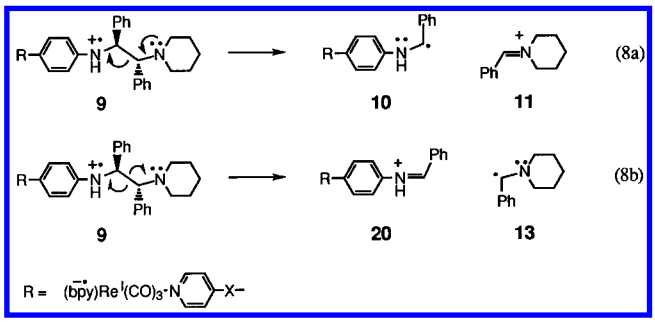

The transient absorption spectra of the radical products produced by C−C bond fragmentation in ***e*-1a** and ***e*-1b** (Figure 3a,b) indicate that heterolytic fragmentation predominates or occurs exclusively. The spectra produced by photolysis of ***e*-1a** and ***e*-1b** exhibit absorption bands with maxima at 365 and 425 nm, respectively. These absorption bands are attributed to the α-amino radical chromophore, $RC_6H_4NH\dot{C}HC_6H_5$,[13b,17,31] which is present in metal complex radicals **10a** and **10b**. The absorption maximum of the $RC_6H_4NH\dot{C}HC_6H_5$ chromophore is red-shifted substantially in **10b** compared to **10a** because of the effect of conjugation between the pyridine and aniline rings. Note that α-amino radical **13**, which would be produced by homolytic fragmentation, exhibits a very strong absorption at $\lambda_{max} \approx 340$ nm.[13b] This band does not appear in the spectra of either ***e*-1a** or ***e*-1b**, as would be expected if homolytic fragmentation occurs.

SCHEME 4

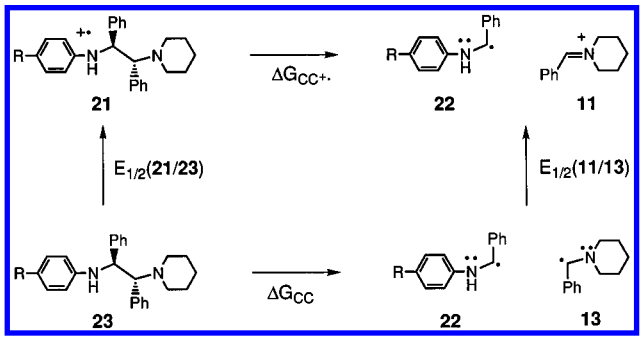

A thermodynamic cycle that can be used to estimate the free energy for fragmentation of diamine radical cation **21** is illustrated in Scheme 4. The free energy can be calculated by eq 9:[32]

$$\Delta G_{CC^{\bullet+}} = \Delta G_{CC} - F[E_{1/2}(\mathbf{11/13}) - E_{1/2}(\mathbf{21/23})] \quad (9)$$

where $\Delta G_{CC^{\bullet+}}$ and ΔG_{CC} are, respectively, the free energies for bond fragmentation of radical cation **21** and the corresponding neutral **23**, the $E_{1/2}$'s represent electrochemical half-wave potentials for the indicated one-electron reductions, and F is the Faraday constant. $E_{1/2}$(**21**/**23**) is given approximately by E_p for ***e*-1a** and ***e*-1b** (+0.85 V), while $E_{1/2}$(**11**/**13**) is available from the literature (−0.94 V).[33] An estimate for ΔG_{CC} is arrived at through the following reasoning. First, the literature value for ΔH_{CC} for the 1,2-CC bond in *N*,*N*,*N*′-trimethyl-1,2-diaminoethane is +60 kcal/mol.[34] Analysis of bond homolysis data for a variety of aryl-substituted ethanes indicates that vicinal diphenyl substitution typically decreases ΔH_{CC} by ≈22 kcal/mol compared to the corresponding ethane.[34] These values lead to an estimate of $\Delta H_{CC} \approx 38$ kcal/mol for ***e*-1a** and ***e*-1b**. Finally, an estimate of $\Delta S_{CC} \approx 36$ eu for ***e*-1a** and ***e*-1b** is based on ΔS_{CC} values for ethane (38 eu), 1,2-diphenylethane (36 eu), and 1,2-diaminoethane (36 eu).[35] By using the estimated values for ΔH_{CC} and ΔS_{CC} for ***e*-1a** and ***e*-1b**, we calculate that ΔG_{CC}(298 K) ≈ +27 kcal/mol.

Substitution of the estimated values for $E_{1/2}$(**21**/**23**), $E_{1/2}$(**11**/**13**), and ΔG_{CC} into eq 9 leads to a calculated value of $\Delta G_{CC}^{\bullet+} = -14 \pm 5$ kcal/mol for **21** (and by analogy for the radical cations of ***e*-1a** and ***e*-1b**), where the estimated error of 5 kcal/mol takes into account errors arising from estimation of ΔG_{CC}(298 K) and from using an irreversible peak potential for ***e*-1a** and ***e*-1b** rather than a reversible potential. The estimate of $\Delta G_{CC^{\bullet+}} \approx -14$ kcal/mol indicates that bond fragmentation of the diamine cation radical is moderately exothermic. In view of this fact, it is remarkable that the reaction is thermally activated: the rate of bond fragmentation at 298 K (3×10^8 s^{-1}) indicates an activation free energy ($\Delta G^{\neq}_{CC^{\bullet+}}$) of +3 kcal/mol. That fragmentation of the diamine cation radical is weakly activated despite being moderately exothermic implies that bond cleavage has an associated "reorganization energy", or intrinsic barrier. This energetic barrier may be due to free energy costs associated with the stereoelectronic demands of the transition state[36,37] and solvent repolarization that occurs along the reaction coordinate. Indeed, the fragmentation kinetics of diastereomeric

aminoalcohol cation radicals (eq 1, X = OH) imply that in the transition state for fragmentation there is a stereoelectronic requirement for maximization of orbital overlap between the p orbital on the heteroatom of the electrofugal group (X in eq 1) and the singly occupied p orbital on N.[14,31] Overlap is maximized if the two heteroatoms are oriented either *syn* or *anti* with respect to rotation about the 1,2-CC bond. It is plausible that the intrinsic barrier for fragmentation of the 1,2-diamine cation radical is due to an unfavorable enthalpy or probability factor (activation entropy) associated with achievement of the proper orbital alignment in the transition state.[36,37]

Mechanism for *e*-1 to *t*-1 Isomerization. One of the surprising outcomes of the photochemical studies of ***e*-1a** and ***e*-1b** is the observation of *erythro* → *threo* photoisomerization. This reaction provides unequivocal evidence that bond fragmentation is reversible, albeit in an operational but not necessarily strictly mechanistic sense, *vide infra*. An important observation is that ***e*-1** → ***t*-1** isomerization is not observed under air-saturated conditions (see Φ_{threo}, Table 2), which indicates that *geminate* recombination of α-amino radical **10** and iminium **11** does not occur. That geminate recombination does not occur implies that direct recombination of **10** and **11** to produce **9** is not feasible.[38] Furthermore, it suggests that recombination requires a preceding ET step from $bpy^{\bullet-}$ in **10** to iminium ion **11** to produce the radicals **12** and **13**, which then recombine (Scheme 3). The thermodynamic driving force for this outer sphere ET reaction is estimated as $\Delta G \approx -0.23$ eV on the basis of the reduction potentials of the coordinated bpy ligand ($E_{1/2} = -1.17$ V, Table 3) and iminium ion **11** ($E_{1/2} \approx -0.94$ V).[33] A subtle, but interesting point to consider is that the lack of geminate recombination indicates that $bpy^{\bullet-}$ to iminium ET does not occur within the geminate pair [**10**,**11**] that is initially produced by C−C bond fragmentation. The lack of ET at this stage may be due to poor electronic coupling between the donor (e.g., $bpy^{\bullet-}$) and the iminium ion, which are likely to be separated by 10−15 Å immediately following bond fragmentation.

Finally, it is important to note that the behavior of metal complexes ***e*-1a** and ***e*-1b** contrasts with that of *free ligand* **6a** and the related diamine **6b**.[17] Compounds **6a** and **6b** undergo 1,2-CC bond fragmentation and *erythro* → *threo* stereoisomerization when irradiated in *air-saturated* solution, presumably via a mechanism involving geminate recombination. However, the mechanism for bond fragmentation in **6a** and **6b** differs in such a way that a radical pair, rather than a radical−ion pair, is produced by bond fragmentation. In this case, recombination directly produces the neutral diamine in a reaction that is exoergonic by ca. 27 kcal/mol (the C−C bond free energy).

Summary and Conclusions

The photophysics and photochemistry of diamine-substituted complexes ***e*-1a** and ***e*-1b** have been carefully examined. Photoexcitation of these complexes affords the LLCT state with high efficiency via a sequence involving initial population of the MLCT state followed by intramolecular diamine donor to metal ET. The diamine radical cation which is present in the LLCT state undergoes irreversible carbon−carbon bond fragmentation with $k_{BF} = 3 \times 10^8\ s^{-1}$, while the LLCT state decays by back ET with $k_{BET} = 1 \times 10^8\ s^{-1}$. Bond fragmentation competes very effectively with back ET in both ***e*-1a** and ***e*-1b**, and as a result, the overall quantum efficiency for irreversible photochemistry of the complexes is high. The surprising observation of *erythro* → *threo* photoisomerization for ***e*-1a** and ***e*-1b** indicates that bond fragmentation is reversible. However, the fact that geminate recombination does not occur leads to the conclusion that recombination does not occur between the primary radical−ion pair formed by fragmentation of the diamine radical cation, but rather involves a two-step sequence involving electron transfer followed by radical−radical recombination.

A primary objective of this study was to develop a reactive donor ligand system which is useful for probing the electronic structure and dynamics of charge transfer excited states in metal complex systems. The 1,2-diamine ligands which provide the basis for the unique reactivity of ***e*-1a** and ***e*-1b** clearly satisfy this objective. Future studies seek to apply the diamine and other reactive donor systems to explore the electronic structure, dynamics, and reactivity of MLCT, LLCT, and ion-pair CT states in inorganic and organometallic complexes.

Acknowledgment. We gratefully acknowledge support for this project from the National Science Foundation (Grant Nos. CHE 91-23000 and CHE-9401620).

Supporting Information Available: HPLC chromatograms for photolyzed solutions of ***e*-1a** and ***e*-1b** under argon-degassed and air-saturated conditions (2 pages). See any current masthead page for ordering information.

References and Notes

(1) (a) Bock, C. R.; Meyer, T. J.; Whitten, D. G. *J. A. Chem. Soc.* **1974**, *96*, 4710. (b) Young, R. C.; Meyer, T. J.; Whitten, D. G. *J. Am. Chem. Soc.* **1975**, *97*, 4782. (c) Bock, C. R.; Connor, J. A.; Guitierrez, A. R.; Meyer, T. J.; Whitten, D. G.; Sullivan, B. P.; Nagle, J. K. *J. Am. Chem. Soc.* **1979**, *101*, 4815.

(2) (a) Sutin, N.; Creutz, C. *J. Chem. Ed.* **1983**, *10*, 809. (b) Marcus, R. A.; Sutin, N. *Biochim. Biophys. Acta* **1985**, *811*, 265.

(3) (a) Scandola, F.; Balzani, V. *J. Chem. Ed.* **1983**, *10*, 814. (b) Juris, A.; Balzani, V.; Barigelletti, F.; Campagna, S.; Belser, P.; Von Zelewsky, A. *Coord. Chem. Rev.* **1988**, *84*, 85.

(4) (a) Hoffman, M. Z. *J. Phys. Chem.* **1988**, *92*, 3458. (b) Ohno, T.; Yoshimura, A.; Prasad, D. R.; Hoffman, M. Z. *J. Phys. Chem.* **1991**, *95*, 4723.

(5) *Photoinduced Electron Transfer*; Fox, M. A., Chanon, M. D., Eds.; Elsevier: Amsterdam, 1988; Parts A−D.

(6) *Photoinduced Electron Transfer II*; Mattay, J., Ed.; *Top. Curr. Chem.* **1990**, *158*, 1−199.

(7) (a) Westmoreland, T. D.; Le Bozec, H.; Murray, R. W.; Meyer, T. J. *J. Am. Chem. Soc.* **1983**, *105*, 3932. (b) Chen, P.; Westmoreland, T. D.; Danielson, E.; Schanze, K. S.; Anthon, D.; Neveaux, P. E., Jr.; Meyer, T. J. *Inorg. Chem.* **1987**, *26*, 1116. (c) Chen, P.; Duesing, R.; Graff, D. K.; Meyer, T. J. *J. Phys. Chem.* **1991**, *95*, 5850. (d) Jones, W. E., Jr.; Bignozzi, C. A.; Chen, P.; Meyer, T. J. *Inorg. Chem.* **1993**, *32*, 1167. (e) Mecklenburg, S. L.; Peek, B. M.; Schoonover, J. R.; McCafferty, D. G.; Wall, C. G.; Erickson, B. W.; Meyer, T. J. *J. Am. Chem. Soc.* **1993**, *115*, 5479.

(8) (a) Elliott, C. M.; Freitag, R. A.; Blaney, D. D. *J. Am. Chem. Soc.* **1985**, *107*, 4647. (b) Cooley, L. F.; Headford, C. E. L.; Elliott, C. M.; Kelley, D. F. *J. Am. Chem. Soc.* **1988**, *110*, 6673. (c) Ryu, C. K.; Wang, R.; Schmehl, R. H.; Ferrere, S.; Ludwikow, M.; Merkert, J. W.; Headford, C. E. L.; Elliott, C. M. *J. Am. Chem. Soc.* **1992**, *114*, 430. (d) Larson, S. L.; Elliott, C. M.; Kelley, D. F. *J. Phys. Chem.* **1995**, *99*, 6530.

(9) (a) Yonemoto, E. H.; Riley, R. L.; Kim, Y. I.; Atherton, S. J.; Schmehl, R. H.; Mallouk, T. E. *J. Am. Chem. Soc.* **1992**, *114*, 8081. (b) Yonemoto, E. H.; Saupe, G. B.; Schmehl, R. H.; Hubig, S. M.; Riley, R. L.; Iverson, B. L.; Mallouk, T. E. *J. Am. Chem. Soc.* **1994**, *116*, 4786.

(10) (a) Fox, L. S.; Kozik, M.; Winkler, J. R.; Gray, H. B. *Science* **1990**, *247*, 1069. (b) Farid, R. S.; Chang, I.-J.; Winkler, J. R.; Gray, H. B. *J. Phys. Chem.* **1994**, *98*, 5176.

(11) Goulle, V.; Harriman, A.; Lehn, J.-M. *J. Chem. Soc., Chem. Commun.* **1993**, 1034.

(12) (a) Schanze, K. S.; Sauer, K. *J. Am. Chem. Soc.* **1988**, *110*, 1180. (b) Schanze, K. S.; Cabana, L. A. *J. Phys. Chem.* **1990**, *94*, 2740. (c) Perkins, T. A.; Hauser, B. T.; Eyler, J. R.; Schanze, K. S. *J. Phys. Chem.* **1990**, *94*, 8745. (d) MacQueen, D. B.; Schanze, K. S. *J. Am. Chem. Soc.* **1991**, *113*, 7470.

(13) (a) Wang, Y.; Hauser, B. T.; Rooney, M. M.; Burton, R. D.; Schanze, K. S. *J. Am. Chem. Soc.* **1993**, *115*, 5675. (b) Wang, Y.; Lucia, L. A.; Schanze, K. S. *J. Phys. Chem.* **1994**, *99*, 1961. (c) Lucia, L. A.; Wang, Y.; Nafisi, K.; Netzel, T. L.; Schanze, K. S. *J. Phys. Chem.* **1995**, *99*, 11801.

(14) Ci, X.; Kellett, M. A.; Whitten, D. G. *J. Am. Chem. Soc.* **1991**, *113*, 3893.
(15) (a) Kellett, M. A.; Whitten, D. G. *J. Am. Chem. Soc.* **1989**, *111*, 2314. (b) Leon, J. W.; Whitten, D. G. *J. Am. Chem. Soc.* **1993**, *115*, 8038.
(16) Wang, Y.; Schanze, K. S. *Inorg. Chem.* **1994**, *33*, 1354.
(17) Wang, Y.; Schanze, K. S. *J. Phys. Chem.* **1995**, *99*, 6876.
(18) (a) Perkins, T. A.; Pourreau, D. B.; Netzel, T. L.; Schanze, K. S. *J. Phys. Chem.* **1989**, *93*, 4511. (b) Wang, Y.; Schanze, K. S. *Chem. Phys.* **1993**, *176*, 305.
(19) Schanze, K. S.; MacQueen, D. B.; Perkins, T. A.; Cabana, L. A. *Coord. Chem. Rev.* **1993**, *122*, 63, and references therein.
(20) Lucia, L. A.; Schanze, K. S. *Inorg. Chim. Acta* **1994**, *225*, 41.
(21) *Encyclopedia of the Electrochemistry of the Elements*; Bard, A. J., Ed.; Marcel Dekker: New York, 1973.
(22) Oevering, H.; Paddon-Row, M. N.; Heppener, M.; Oliver, A. M.; Cotsaris, E.; Verhoeven, J. W.; Hush, N. S. *J. Am. Chem. Soc.* **1987**, *109*, 3258.
(23) An interesting point is that while 366-nm excitation of ***e*-1a** directly populates the dπ (Re) $\rightarrow \pi^*$ (bpy) MLCT manifold, 366-nm excitation of ***e*-1b** must lead initially to a state having substantial π,π^* IL-CT character. Despite this difference, two features indicate that the reactivity of ***e*-1b** emanates from a state having diamine donor $\rightarrow \pi^*$ (bpy) LLCT character, and not one having π,π^* IL-CT character. First, the reactivity of ***e*-1a** and ***e*-1b** are nearly identical, in both qualitative and quantitative sense. Second, C−C bond fragmentation is nearly 8-fold more efficient in ***e*-1b** than in the free ligand **6b**.[17]
(24) The assumption that k_{BF} is the same for ***e*-1a** and ***e*-1b** is supported by a recent unpublished study we carried out which examined the relationship between the oxidation potentials ($E_{1/2}$(ox)) for a series of aminoalcohols and the rate of C−C bond fragmentation (k_{BF}) for the corresponding aminoalcohol radical cations. This study indicated that there is an *excellent* correlation between log k_{BF} and $E_{1/2}$(ox) for the series. Since the oxidation potentials of the diamine ligands in ***e*-1a** and ***e*-1b** are the same within experimental error, the aforementioned correlation suggests that k_{BF} will be the same for the two diamine radical cations.
(25) Equation 5a assumes that the lowest MLCT excited state is populated with unit quantum efficiency following excitation.
(26) The difference in electronic coupling between two aromatic rings which are directly attached (e.g., conjugated) or separated by a single methylene spacer is examplified by studies of the intensity of intervalence charge transfer absorption bands in mixed-valence complexes of the type $(NH_3)_5Ru^{II}-L-Ru^{III}(NH_3)_5^{3+}$, where L = 4,4′-bipyridine or bis(4-pyridyl)-methane. The electronic coupling matrix element is ca. 10 fold times larger in the 4,4′-bipyridine bridged complex compared to that of the bis(4-pyridyl)-methane complex.[27]
(27) (a) Fischer, H.; Tom, G. M.; Taube, H. *J. Am. Chem. Soc.* **1976**, *98*, 5512. (b) Rieder, K.; Taube, H. *J. Am. Chem. Soc.* **1977**, *99*, 7891.
(28) Wasielewski, M. R. *Chem. Rev.* **1992**, *92*, 435.
(29) Striplin, D. R.; Crosby, G. A. *Chem. Phys. Lett.* **1994**, *221*, 426.
(30) (a) Steiner, U. E.; Wolff, H.-J.; Ulrich, T.; Ohno, T. *J. Phys. Chem.* **1989**, *93*, 5147. (b) Wolff, H.-J.; Bürssner, D.; Steiner, U. E. *Pure Appl. Chem.* **1995**, *67*, 167.
(31) Lucia, L. A.; Burton, R. D.; Schanze, K. S. *J. Phys. Chem.* **1993**, *97*, 9078.
(32) Wayner, D. D. M.; Parker, V. D. *Acc. Chem. Res.* **1993**, *26*, 287.
(33) (a) Andriux, C. P.; Saveant, J. M. *Bull. Soc. Chim. Fr.* **1968**, 4671. (b) Andriux, C. P.; Saveant, J. M. *J. Electroanal. Chem.* **1970**, *26*, 223.
(34) McMillin, D. F.; Golden, E. M. *Annu. Rev. Phys. Chem.* **1982**, *33*, 493.
(35) Stein, S. E.; Rukkers, J. M.; Brown, R. L. NIST Standard Reference Data No. 25, Computer Program for MS-DOS, Version 1.2, 1991.
(36) Bellville, D. J.; Pabon, R. A.; Bauld, N. L. *J. Am. Chem. Soc.* **1985**, *107*, 4978.
(37) Camaioni, D. M. *J. Am. Chem. Soc.* **1990**, *112*, 9475.
(38) Note that the thermochemical cycle (Scheme 4) indicates that direct recombination of metal complex radical **10** and iminium **11** is *endoergonic* by ca. 14 kcal/mol.

JP953537L